Estimation of Chirp Sonar Signal Attenuation for Classification of Marine Sediments : Improved Spectral Ratio Method

C. S. Maroni, A. Quinquis

ENSIETA
Dpt EIA
2, rue François Verny
29806 Brest Cedex 9, France
E-mail: maronicl@ensieta.fr

Abstract

Remote sediment classification through acoustic methods is of great interest for a few years . The attenuation coefficient of the transmitted wave is an important feature to characterize physical sediment layers properties. Hence, an improved spectral ratio method for the estimation of the chirp sonar signal attenuation is proposed in the paper. A new time-frequency based on technique to compute the least square line is outlined. Finally, the method is tested on synthetic data and some results are discussed.

1. Introduction

Remote sediment classification through acoustic methods has the potential to reduce the cost and effort that current methods require using coring for seafloor classification. But over the past two decades of marine subbottom exploration, the reflection profiling technique has been used primarily to delineate geological and stratification structures. To date, seafloor properties have been determined by sampling the sediment followed by laboratory analyses. This process not only fails to obtain undisturbed samples but also is extremely slow, very expensive, and provides information only at discrete sites. A remote acoustic sediment classification system would eliminate most of the present needs for sediment sampling, while generating continuous profiles of sediment properties. A quantitative analysis of the reflected signal to characterize subsurface sediments is proposed for a few years, but it is still far from being effective in practice.

The attenuation coefficient can be used to classify sediments and to estimate physical sediments properties. Several attenuation measurement techniques have been proposed both in the time and frequency domains : rise-time, spectral ratio, spectral shift, and matched filtering [1] [2]. For the spectral ratio method, overlapping reflections produce errors in the spectral estimates of the different echos. That's why we propose in this paper a new approach to improve results yielded by this classical method.

The subbottom profiler used, transmits a FM pulse, that is linearly swept from 4.5 kHz to 2.5 kHz during 25 ms. This pulse is compressed using a matched filter which correlates the return signal with a replica of the outgoing FM pulse. Owing to a 2 kHz frequency bandwidth, the compressed chirp width is 0.5 ms, which provides a forty centimeters vertical resolution. It's a monostatic configuration in normal incidence.

2. Classical Spectral Ratio Method

2.1. Sea bottom model

The sea bottom is modeled as a layered medium. Unlike the Goupillaud model [3], the one way travel-time in each layer need not be equal. The assumption involved are:

1. The layers are parallel and laterally homogeneous. Normally, this can be quantified in terms of the roughness scale, which should not be greater than the $\frac{1}{4}$ wavelength measured at the central frequency of the FM pulse.
2. The interface reflection coefficients are frequency independent.
3. Phase dispersion and pulse spreading due to attenuation can be neglected. However, the loss of signal energy due to attenuation is accounted for in the model.
4. The acoustic wave travels through the layers as a plane wave at normal incidence. The reflected signal can be written as the convolution of the source signal with the impulse response of the medium.

2.2. Attenuation model

When the sonar pulse travels through an absorbent sea bottom, its energy is reduced in several ways. All the mechanisms lead to the attenuation coefficient α. Attenuation will cause the amplitude of a plane wave to fall off exponentially with the distance traveled. The pulse amplitude losses are evaluated by $\exp(-\alpha\tau)$, where τ is the traveling time.
Hamilton [4] has compiled an important part of the available data published on sea bottom effective attenuation. This author concludes that α varies linearly with frequency. If this assumption was sometimes debated, it is usually allowed in this frequency range. Hence, α can be written as follows :

$$\alpha(f) = \frac{1}{8,686} \times \beta \times \tau \times f \tag{1}$$

Note that β is the attenuation coefficient of the compressional wave in dB/wavelength ($8.686 = 20\log_{10}(e)$). Typical values of β range from 0.1 to 1.0 dB/wavelength. Let us consider a medium with two sediments layers, and assume that the second one is semi-infinite. In other words, the lower bound interface of the second layer, is not caught by the sonar, because of sediment attenuation and layer thickness. Reflected signal in the frequency domain, can be written :

$$\begin{aligned} Y(f) &= R_{12} \times S(f) + T_{12}R_{23}T_{21}\exp(j\tau\omega)\exp\left(-\frac{\beta\ \tau\ f}{8,686}\right) \times S(f) \\ &= A_1(f) + A_2(f)\exp(j\tau\omega) \end{aligned}$$

where $A_1(f)$ and $A_2(f)$ are the amplitude spectra of the seabed echo(reflected by the water-sediment interface) and the first reflector (reflected by the interface between the first and the second subbottom layer). Hence we infer the equation (2) that links together the spectral contributions of the two echos.

$$A_2(f) = G \times A_1(f) \times \exp\left(-\frac{\beta \times f \times (t_2 - t_1)}{8.686}\right) \tag{2}$$

where f stands for frequency, $t1$ and $t2$ are respectively the locations of the seabed and the first reflector echoes, and $\tau = t_2 - t_1$. G is a frequency independent factor that allows for change in pulse magnitude due to reflection and transmission coefficients (R_{12}, R_{23}, T_{12} and T_{21}).

2.3. Estimation technique

Equation (2) can be rewritten as (3), taking the logarithm of the Spectral Ratio$A_2(f)/A_1(f)$

$$\ln\frac{A_2(f)}{A_1(f)} = \ln(G) - \beta \times \frac{(t_1 - t_0)}{8.686} \times f \tag{3}$$

The linear dependence of $\ln A_2(f)/A_1(f)$ versus frequency makes possible the attenuation coefficient (β) estimation, by simply plotting the left side of equation (3) versus frequency. The least squares line fitted through the plotted data yields an estimation of the attenuation coefficient β, because $t1$ and $t2$ can be estimated from the peaks of

the reflected signal envelope, after the matched filtering.
This method provides good results if pulse reflections produced by sediment layers are well separated, allowing good spectral estimation for $A_1(f)$ and $A_2(f)$. With a 25 ms pulse width, the first layer thickness should be larger than 19 m $(25.10^{-3} * 1500/2)$ to avoid overlapping of the two echoes. Fortunately the reflected signals are processed by matched filtering so that the compressed chirp width is 1 ms. Good estimation of β can then be expected, for a delay between the two echoes larger than 1 ms. But, as we will see in the simulation results section, the spectral information of the first reflector is corrupted by the presence of the reflection on the seabed a few ms before. In fact, although the side lobes are very small with respect to the correlated signal main lobe, their influence disturbs the spectrum estimation. Also bad estimations of $A_2(f)$ can provide for β a value which is really different from the real one. That's why an improved spectral ratio method is proposed.

3. Improved Spectral Ratio method

In order to improve the previously presented method, we develop a time-frequency analysis of the compressed chirp, and prove that overlapping reflections produce disturbance only in a limited frequency band.

3.1. Time-frequency analysis of the correlated signal

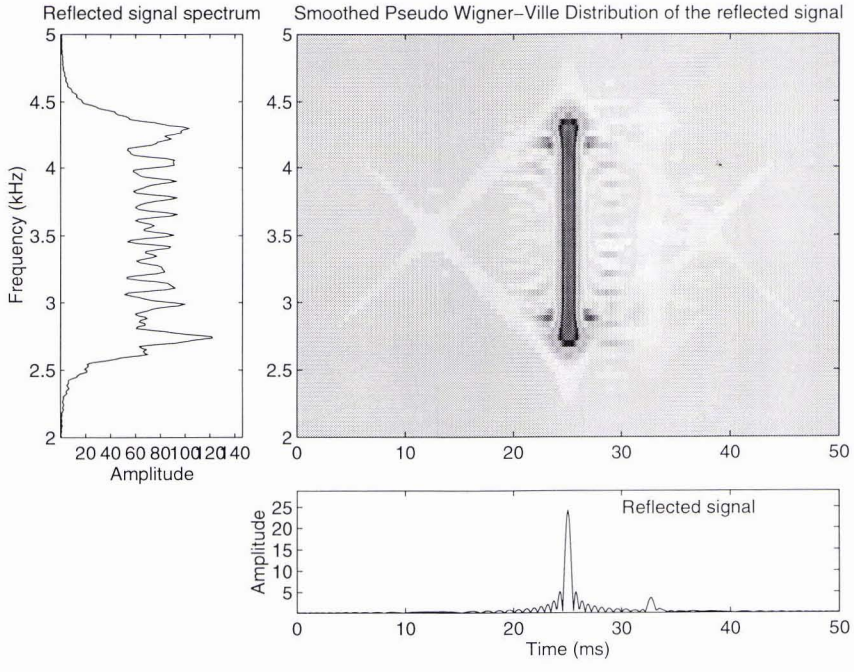

Figure 1: Reflected signal representations in time, frequency and time-frequency domains

Different properties of a signal are revealed if it is represented in the time or in the frequency domain. But the most complete manner for the visualization of its behaviour is the time-frequency analysis. For instance, this is particularly adapted to subbottom echoes, because it can display the evolution of the frequency content versus time, i.e., versus propagation distance, which does not appear when classical spectral analysis is used.
A lot of time-frequency analysis tools was developed in the last few decades. Among them, the Wigner-Ville distribution is a quite powerful instrument with excellent properties concerning the temporal and frequency support preservation and the compatibility with the filtering and modulation operators. It is defined [5] by:

$$WD_s(t,\nu) = \int_{-\infty}^{+\infty} s(t+\frac{\tau}{2})\ s^*(t-\frac{\tau}{2})\ e^{-j2\pi\nu\tau} d\tau \tag{4}$$

where s(t) is the original signal. Its popularity among the Cohen's class distributions is due to the fact that it achieve the best trade-off between the temporal and frequency resolution for a given signal and it allows an exact pursuit of the CHIRP instantaneous frequency.
Its main disadvantage concerns the existence of the cross components which can lead to difficulties of interpretation. Hence, a modified version, named Smoothed Pseudo Wigner-Ville distribution (SPWD) given by:

$$SPWD_s(t,\nu) = \int_{-\infty}^{+\infty} h(\tau) \int_{-\infty}^{+\infty} g(t-u)\ s(u+\frac{\tau}{2})\ s^*(u-\frac{\tau}{2})\ du\ e^{-j2\pi\nu\tau} d\tau \tag{5}$$

has been used in the paper. The introduction of the two windows, h and g, leads to a smoothing of the cross components in the time-frequency domain. In order to improve the legibility of the time-frequency image, the following parameter s have been used: FFT length: 128 points, window type: Hamming, h window length: 128 points, g window length: 33 points, with a 12 kHz sampling frequency.
The figure 1 shows the SPWD of the CHIRP correlated signal reflected by two layers subbottom. Note that the two CHIRP components corresponding to the two reflections are well pursuited and the two correlation maxima are well localized. This image will be used in the section 3.3. to describe the improved spectral ratio method principle.

3.2. Analytical expression of the correlated signal

The autocorrelation function of the signal s(t) is given by:

$$\Gamma_s(\tau) = \int_0^{T-\tau} s(t)\ s(t+\tau)\ dt, \qquad 0 \le \tau \le T \tag{6}$$

with

$$\Gamma_s(\tau) = \Gamma_s(-\tau)$$

where the CHIRP signal expression is:

$$s(t) = \cos\left(\omega_0 t + \frac{\mu t^2}{2}\right), \qquad 0 \le t \le T \tag{7}$$

Consequently:

$$\begin{aligned}
\Gamma_s(\tau) &= \int_0^{T-\tau} cos\left(\omega_0 t + \frac{\mu t^2}{2}\right) cos\left(\omega_0 (t+\tau) + \frac{\mu\ (t+\tau)^2}{2}\right)\ dt \\
\Gamma_s(\tau) &= I_1 + I_2 \\
&\quad where\ : \\
I_1 &= \frac{1}{2}\int_0^{T-\tau} cos\left(\omega_0\tau + \mu\ \tau\ t + \frac{\mu\tau^2}{2}\right)\ dt \\
I_2 &= \frac{1}{2}\int_0^{T-\tau} cos\left(2\omega_0 t + \omega_0\tau + \mu\ t^2 + \mu\ \tau\ t + \frac{\mu\tau^2}{2}\right)\ dt
\end{aligned}$$

It was found that for compression ratios larger than 30, that is the case of this work, I_2 can be neglected. Therefore:

$$\Gamma_s(\tau) = cos\left(\left[\omega_0 + \frac{\mu\ T}{2}\right]\tau\right)\left[\frac{sin\left(\frac{\mu\ \tau\ (T-\tau)}{2}\right)}{\frac{\mu\ \tau\ (T-\tau)}{2}} \times \frac{T-\tau}{2}\right] \tag{8}$$

which can be expressed also as:

$$\begin{aligned}
\Gamma_s(\tau) &= \frac{1}{2}\frac{sin\left(\omega_0\tau + \mu\ \tau\ (T-\tau) + \frac{\mu\tau^2}{2}\right) - sin\left(\omega_0\tau + \frac{\mu\tau^2}{2}\right)}{\mu\tau} \\
&= \frac{1}{2}\frac{sin\left(\omega_0\tau + \mu\ \tau\ T - \frac{\mu\tau^2}{2}\right) - sin\left(\omega_0\tau + \frac{\mu\tau^2}{2}\right)}{\mu\tau}
\end{aligned} \tag{9}$$

The former equation (8) is the well known expression of the correlated signal and it highlights the 'sinc' envelope and the oscillating component at the central frequency :

$$\nu_c = \frac{\omega_0 + (\mu\ T)/2}{2\pi} = 3.5\ kHz$$

This is the most commonly considered expression of the correlated signal when the CHIRP signal is used. However, for the time-frequency analysis, it is more interesting to consider the second expression (9), which shows that the correlated signal can be viewed as the superposition of the two CHIRP having opposed frequency variation slopes. The interpretation of the figure 1 can be now readily done.

3.3. Attenuation coefficient estimation

A simplified representation of the Smoothed Pseudo Wigner Ville Distribution of the reflected signal 1, is displayed on figure 2.

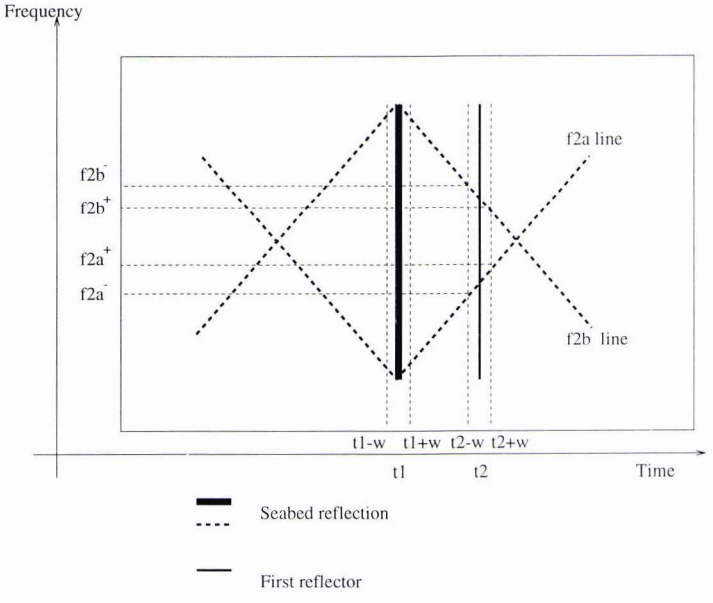

Figure 2: Simplified representation of the reflected signal SPWD

Note that, around $t2$, the spectrum of the signal will be composed of two contributions : the former (the vertical one) provided by the reflector, and the second one due to the presence of two oblique lines. These latter correspond to the two chirps, that were highlighted in previous section, and whose equations are given by

$$f2_a(\tau) = \frac{1}{2\pi}\frac{d}{dt}(\omega_0\tau + \mu\ \tau\ T - \frac{\mu\tau^2}{2}) \quad (10)$$

$$f2_b(\tau) = \frac{1}{2\pi}\frac{d}{dt}(\omega_0\tau + \frac{\mu\tau^2}{2}) \quad (11)$$

where $\tau = t - t1$, or in others words, $t1$ time arrival of the seabed reflection, is the time origin. Equations (10) and (11) become :

$$f2_a(\tau) = 2.5 + 80 \times \tau\ in\ kHz \quad (12)$$

$$f2_b(\tau) = 4.5 - 80 \times \tau\ in\ kHz \quad (13)$$

by substituting parameters with their numerical values, corresponding to the EPSHOM subbottom profiler used, i.e $T = 25\ ms$, $f_0 = 4500\ Hz$, and $\Delta f = -2\ kHz$ $\mu = 2\pi\frac{\Delta f}{T} = -2\pi \times 80000$ Note that for the subbottom profiler used, $\mu =< 0$. We are dealing therefore with a decreasing frequency modulation. Hence, the frequencies affected by the previous reflection, can be estimated after τ estimation. More precisely, not only two frequencies are disturbed, but two little frequency bands. Actually, in order to estimate $A1(f)$ and $A_2(f)$, a Nw-point rectangular window centered on the envelope peaks, is used (Nw=2*w+1, see figure 2). So we have to compute :

$$f2_a^- = f2_a((t2 - w) - t1) \quad (14)$$

$$f2_a^- = f2_a((t2 + w) - t1) \quad (15)$$

$$f2_b^- = f2_b((t2 - w) - t1) \quad (16)$$

$$f2_b^+ = f2_b((t2 + w) - t1) \quad (17)$$

Afterwards, $\ln A_2(f)/A_1(f)$ is computed, but the least squares line calculation takes now into account in a different manner the part of the frequency band which is affected by perturbation and the valid part. That means that we not longer consider $\ln A_2(f)/A_1(f)$ values for $f\epsilon[f2_a^-, f2_a^-] \cup [f2_b^-, f2_b^+]$, when the least squares line is computed.

4. Simulation results

We test our method on synthetic data generated with the model proposed in section 2.. Four sediment types are considered, for the first layer : silt, fine sand, sand and gravel. For the second layer, rock is also proposed. Sediment and rock acoustical parameters used [6] are presented in table 1. More precisely, parameters presented in this table, are central parameters of each type of sediment, and we usually consider an interval around this central value. For each class the first layer is fixed, until the second layer fluctuates as shown in table 2.

	Silt	Fine Sand	Sand	Gravel	Rock
Density (g/cm^3)	1.5	1.75	1.95	2	2.6
Celerity (m/s)	1520	1650	1750	2200	4000
Attenuation (dB/lambda)	0.15	0.20	0.8	0.5	

Table 1: Sediment acoustical parameters used for generating reflected signals

	First layer	**Second layer**
Classe1	Silt	Fine sand Sand Gravel Rock
Classe2	Fine sand	Sand Gravel Rock
Classe3	Sand	Gravel Rock
Classe4	Gravel	Rock

Table 2: Different subbotom types considered when testing estimation methods

Both classical and improved Spectral Ratio Method are tested on these different subbottom. Firstly, the subbottom composition is fixed, and only the time interval τ between the two reflections is varied. That means that attenuation coefficient is estimated for various first sediment layer thickness. Figure 3 displays an example of these graphs for each class. The display has been limited to a 0.2 error, because we considered that extra error values were too large. It's readily seen that estimation error provided by the second method is smaller than that provided by the former one. In order to take into consideration the random fluctuation of layer thickness between successive shots, these graphs have been moving average filtered.
Secondly, for fixed τ value, the attenuation coefficient is computed for different subbottoms. Results are presented on figure 4. The dotted curve stands for theoretical attenuation value, until the solid and the dashed plots represent the first and respectively the second attenuation estimation method. The four regions of these graphs correspond to four different theoretical attenuation values of the first subbottom layer. For each of them, second layer features

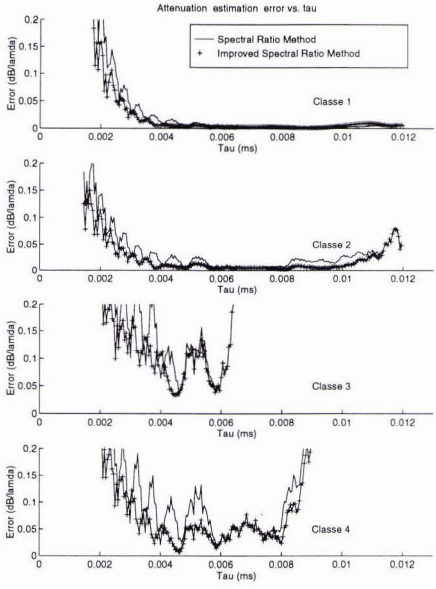

Figure 3: Estimation error ($|\beta_{estimated} - \beta_{theoritical}|$), with the spectral ratio method (solid line) and with the proposed method(++). Each subplot stands for a class of subbottom type.

have been varied to better match practical situations. In any case the proposed method leads an improvement of the attenuation estimation. In addition, the estimation is less sensitive to the second layer type, because in each region, the solid line decreases progressively with the second layer variation, until the dashed line is nearly horizontal.

5. Conclusions

In the case of overlapping reflections, bad attenuation coefficient estimations are provided by the classical Spectral Ratio Method. To overcome this difficulty,a time-frequency analysis of the compressed chirp is developed , and it is proven that overlapping reflections produce disturbances only in limited frequency bands, whose positions depend on the traveled time between echoes. Hence, we have proposed to modify the estimation method, taking into account in a different manner the frequency bands that are affected by perturbation, and the valid ones. This approach was tested on synthetic data, and results were compared with those of the classical one. The estimation is not yet valid in any case, nevertheless the error is appreciably reduced. We plan to extend this improvement on real data. Other time-frequency methods are also being considered in order to relieve the spectral estimations of the other echoes influence, by separating the two echoes before the matched filter processing.

Acknowledgment

We would like to thank SHOM (Brest, France), which supported this work, for supplying real subbottom profile. We are also greatful to Emmanuel Radoi for his support and technical discussions.

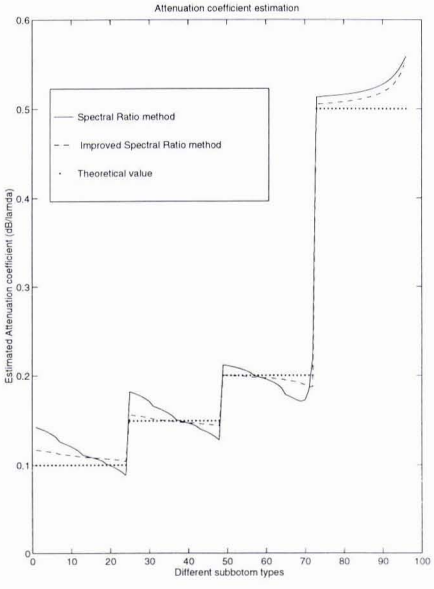

Figure 4: β estimation with both classical and proposed spectral ratio method.

References

[1] D. Jannsen, J. Voss, and F. Theilen, "Comparaison of method to determine q in shallow marine sediments from vertical reflection seismograms," *Geophysical Prosepecting*, vol. 33, pp. 479–497, 1985.

[2] R. Kuc, "Estimating acoustic attenuation from reflected ultrasound signals: Comparaison of spectral-shift and spectral difference approaches," *IEEE Transactions on Acoustics Speech and Signal Processing*, vol. ASSP-2(1), pp. 1–6, 19984.

[3] P. L. Goupillaud, "An approach to inverse filtering of near surface layer effects from seismic records," *Geophysics*, vol. 26, pp. 754–760, 1961.

[4] E. Hamilton, "Geoacoustic modeling of the sea floor," *J. Acoust. Soc. Am*, vol. 68, pp. 1313–1340, 1980.

[5] P. Flandrin, *Temps-Fréquence*. Traité des Nouvelles Technologies, Série Traitement du signal, 14, rue Lantiez, 75017 Paris: Hermes, 1993.

[6] E. Pouliquen, *Identification des fonds marins superficiels à l'aide de signaux d'écho-sondeurs*. Thèse de doctorat, Université Denis Diderot (Paris 7), 1992.